Robotica: (2020) volume 38, pp. 983–999. © Cambridge University Press 2019
doi:10.1017/S026357471900119X

Tri-Criteria Optimization Motion Planning at Acceleration-Level of Dual Redundant Manipulators

Zhaoli Jia†‡, Siyuan Chen¶, Zhijun Zhang¶*, Nan Zhong†*, Pengchao Zhang§, Xilong Qu‖, Jinhua Xie¶ and Fan Ouyang†

†*College of Engineering, South China Agricultural University, Guangzhou 510642, China. E-mails: jiazhaoli0810@163.com, ouyangfan@scau.edu.cn*
‡*Research and Development Center, Guang Dong Siwun Logistics Equipment Co., Ltd, Guangzhou 510507, China*
¶*School of Automation Science and Engineering, South China University of Technology (SCUT), Guangzhou 510641, China. E-mails: c.sy05@mail.scut.edu.cn, 915887584@qq.com*
§*Key Laboratory of Industrial Automation of Shaanxi Province, Shaanxi University of Technology, Hanzhong, Shaanxi 723000, China. E-mail: snutzpc@126.com*
‖*School of Information Technology and Management, Hunan University of Finance and Economics, Changsha, Hunan 410205, China. E-mail: quxilong@126.com*

(Accepted June 24, 2019. First published online: July 23, 2019)

SUMMARY
In order to solve joint-angle drift problem of dual redundant manipulators at acceleration-level, an acceleration-level tri-criteria optimization motion planning (ALTC-OMP) scheme is proposed, which combines the minimum acceleration norm, repetitive motion planning, and infinity-norm acceleration minimization solutions via weighting factor. This scheme can resolve the joint-angle drift problem of dual redundant manipulators which will arise in single criteria or bi-criteria scheme. In addition, the proposed scheme considers joint-velocity joint-acceleration physical limits. The proposed scheme can not only guarantee joint-velocity and joint-acceleration within their physical limits, but also ensure that final joint-velocity and joint-acceleration are near to zero. This scheme is realized by dual redundant manipulators which consist of left and right manipulators. In order to ensure the coordinated operation of manipulators, two motion planning problems are reformulated as two general quadratic program (QP) problems and further unified into one standard QP problem, which is solved by a simplified linear-variational-inequalities-based primal-dual neural network at the acceleration-level. Computer-simulation results based on dual PUMA560 redundant manipulators further demonstrate the effectiveness and feasibility of the proposed ALTC-OMP scheme to resolve joint-angle drift problem arising in the dual redundant manipulators.

KEYWORDS: Joint-acceleration; Joint-velocity; Dual redundant manipulators; Acceleration-level tri-criteria optimization motion planning (ALTC-OMP); Quadratic programming; S-LVI-PDNN.

1. Introduction

With the development of the industrialization, robots have been applied to every aspect of people's lives, such as manufacturing production,[1–3] application in medical machinery,[4] exploring unpredictable regions,[5] and working in hazardous or rough-and-tumble environments.[6–8] In order to satisfy

* Corresponding author. E-mails: auzjzhang@scut.edu.cn, zhongnan@scau.edu.cn

the requirements of mechanical arms motion in different situations, highly efficient, intelligent, and flexible redundant manipulators have been widely studied by scholars.

The traditional robotic manipulators have limited joints and thus usually lacks flexibility, which would lead to a problem that it can only accomplish the main tasks but without subtasks at the same time. Thus the redundant robotic manipulators were proposed and studied. Compared with traditional robotic manipulators, redundant robotic manipulators are more flexible due to their redundant degree of freedoms (DOFS). While executing the main given end-effector task, the redundant robotic manipulators can avoid environment obstacles,[9–13] joint physical limits,[14,15] and singularities.[16] In some complex tasks, such as handling heavy objects, assembling complex parts, and cooking, dual manipulators can complete the aforementioned tasks well while single manipulator cannot. The research of dual redundant manipulators has become a hot topic in the recent years.[17]

In order to achieve more functions of redundant manipulators, motion planning and control methods scheme play an important role in the process of the redundant manipulators application. The solution to motion planning of redundant manipulators is generally obtained by solving their inverse kinematics problem. However, in the process of solving inverse kinematics problem, there will be multiple solutions due to its redundancy. To solve this inverse kinematics problem, many methods were proposed in the recent years.[18–25] The traditional method was pseudo-inverse formulation, which included a specific minimum norm solution and a homogeneous solution.[19,20] This method needs to calculate the pseudo-inverse matrix, which was complicated and time-consuming. At the same time, the traditional method results in non-repeated problems (i.e., the joint angle may not return to its initial state when the end-effector completes a closed path)[21–23] and it did not consider the inequality constraints. In order to overcome these shortcomings, more and more optimal solutions for redundant manipulators were presented, such as minimum-velocity-norm (MVN) scheme,[26] infinity-norm velocity minimization (INVM) scheme,[27] minimum acceleration norm (MAN) scheme,[28] infinity-norm acceleration minimization (INAM) scheme,[29] and infinity-norm torque minimization scheme.[30]

It is worth noting that the schemes mentioned above only consider single criterion at velocity level or acceleration-level. With the deepening of research, single criterion optimization cannot meet the needs in complex environment. Multi-criteria optimization have been proposed by more and more scholars: considering the minimum velocity and INAM, Zhang et al. presented a different-level bi-criteria minimization scheme;[31] and considering the INVM and minimum velocity, Zhang et al. presented MVN-INVM scheme.[32] Liu et al. presented bi-criteria torque optimization based on the dual neural network.[33,34] Liao et al. presented bi-criteria minimization scheme based on the Pseudoinverse-type.[35]

These schemes are effective and feasible when the single manipulator performs simple tasks, but they cannot meet the requirements of multi-manipulator coordinated operation. The optimization scheme of dual manipulators is drawing the attention of more and more scholars. Solving the coordinated motion planning of dual manipulators is a difficult problem. The classical methods to solve coordinated operation motion of dual-robotic manipulators[36] are force control,[37,38] impedance method,[39] and intelligent control method.[40] In the field of the force control, Tsuji et al. presented an algorithm for generating a variety of movements from planning trajectories. That algorithm can satisfy the conditions expressed in terms of gravitational, frictional, and inertial forces.[37] In the field of the impedance method, Heli et al. established a dual-arm of the master-slave motion control method through analyzing the movement characteristics of the research of human arms handling object.[39] In the field of the intelligent control method, Kao et al. designed a two-wheel mobile manipulator with web camera to make it a more home-service robot.

In the recent years, coordinated motion planning of dual manipulators has been widely studied.[30,41–47] Tsai[43] proposed Configuration Time-Rapidly-exploring Random Trees (CT-RRTs) (Bi-direction RRTs in Configuration Time space) algorithm in the structural space, combined the time information to plan the motion of the dual-arm robot, and studied the obstacle avoidance between the two arms by controlling the time of the two arms. Chen[44] presented a search-based motion planning algorithm and made a research and experiment on the dual-arm object manipulation with an upright orientation constraint. That scheme did not consider the repetitive motion condition in the practical application. In the practical application, the relationship between the final position and the initial position should be considered (the ideal state is: the terminal position coincides with the initial position). Zhang et al. presented tri-criteria optimization coordination motion scheme at the

https://doi.org/10.1017/S026357471900119X Published online by Cambridge University Press

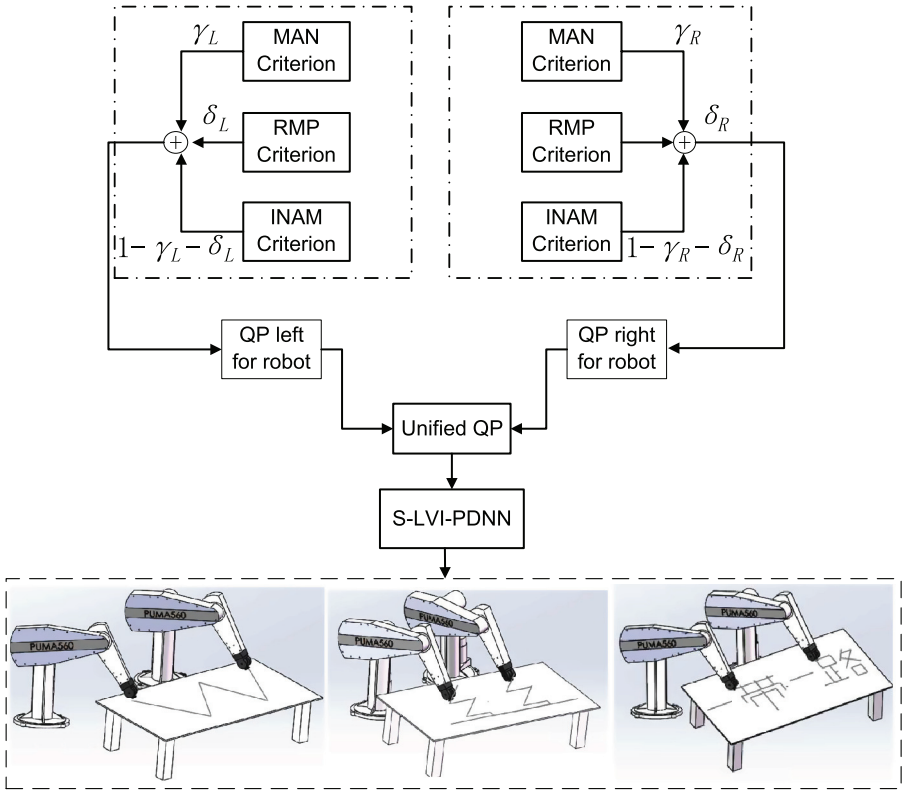

Fig. 1. The diagram of ALTC-OMP scheme for dual redundant manipulators motion control.

velocity level.[48] Some robots need to be controlled and studied in the acceleration layer or in the moment layer. Zhang et al. proposed repetitive motion planning (RMP) of two redundant robot arms at acceleration-level, which did not consider the inequality constraint.[49] Considering the inequality constraint, Zhang et al. proposed the cyclic motion generation scheme at acceleration-level.[50] In this scheme, only a single index is used. Most of the existing motion planning methods for redundant manipulators only consider single-criterion or bi-criteria, which are not flexible enough and are difficult to be used to the robot controlled at acceleration-level. In order to remedy the joint-angle drift, avoid the occurrence of high joint-velocity or high joint-acceleration during the task duration, and achieve a smoother coordination repeated motion operation of dual redundant manipulators at the acceleration-level, an acceleration-level tri-criteria optimization motion planning (ALTC-OMP) scheme has been proposed in this paper. The structural representation of the proposed ALTC-OMP scheme is shown in Fig. 1.

As can be seen from Fig. 1, the mentioned joint-angle drift problem of dual redundant manipulators can be divided into two subproblems, and then two subproblems are formulated into two general quadratic program (QP) problems respectively and further unified into one standard QP problem. Finally the unified QP problem is solved by a simplified linear-variational-inequalities-based primal-dual neural network (S-LVI-PDNN) solver.

This paper is divided into five sections. In the second section, important preliminaries are presented and the joint-angle problem is described as two QP subproblems (i.e., for the left manipulator and the right manipulator respectively). In the third section, the two QP subproblems are unified in one standard QP problem at the acceleration-level and the S-LVI-PDNN solver is proposed to solve the unified standard QP problem. In the fourth section, three path-tracking results (i.e., English letter "W," Chinese characters "silk," and "one belt one road") are illustrated. In the fifth section, the conclusions are drawn with some final remarks. Before ending this section, the main contributions of this paper are summarized as follows:

1. An ALTC-OMP scheme is proposed to remedy the joint-angle drift phenomenon in the redundant manipulators. At the same time, the joint-angle physical limits, joint-velocity physical limits,

https://doi.org/10.1017/S026357471900119X Published online by Cambridge University Press

and joint-acceleration physical limits are considered in the proposed ALTC-OMP scheme. The proposed scheme can solve the joint-angle drift problem of dual redundant manipulators and guarantee joint-angle, joint-velocity, and joint-acceleration within their physical limits. In addition, the proposed ALTC-OMP scheme can guarantee final joint-velocity and joint-acceleration of the motion near to zero, respectively.
2. The proposed ALTC-OMP scheme consisted of two subschemes (i.e., subscheme for the left manipulator and subscheme for the right manipulator), which are reformulated as two subquadratic programs. The two subproblems are formulated into two general QP problems and further unified into one standard QP problem. Finally the unified QP problem is solved by an S-LVI-PDNN solver.
3. The end-effector path tracking of the English letter W, Chinese character of silk, and Chinese characters of one belt one road are designed and served as given tracking task on PUMA560 redundant manipulators.
4. A series of computer simulations by different path-tracking task (i.e., English letter W, Chinese character of silk, and Chinese characters of one belt one road) are executed. Furthermore, two traditional schemes (i.e., MAN scheme and MAN-INAM scheme) are used to finish the same tracking task as comparisons and the results verify the superiority of the proposed ALTC-OMP scheme.

2. Preliminaries and problem formulation

In this section, some fundamental kinematics equations for redundant manipulators are given for the convenience of derivation. Besides, the joint-angle problems are formulated into two QP subproblems based on the given fundamental kinematics equations.

2.1. Preliminaries

First, the classic formulas for the redundant manipulators are presented in this paper as follows:[51,52]

$$r(t) = f(\theta(t)) \tag{1}$$

$$J(\theta(t))\dot{\theta}(t) = \dot{r}(t) \tag{2}$$

$$J(\theta(t))\ddot{\theta}(t) = \ddot{r}(t) - \dot{J}(\theta(t))\dot{\theta}(t) \tag{3}$$

where t, $r(t) \in R^m$, and $\theta(t) \in R^n$ denote time, end-effector position vector, and joint variable vector, respectively. It is worth pointing out that n and m denote the dimensionality of joint space and the dimensionality of task space. $f(\cdot)$ is a differentiable nonlinear function determined by the structure and parameters of the redundant manipulators. $\dot{r}(t)$ and $\ddot{r}(t)$ are respectively the first-order derivative and second-order derivative of $r(t)$. Similarly, $\dot{\theta}(t)$ and $\ddot{\theta}(t)$ are respectively the first-order derivative and second-order derivative of $\theta(t)$. $J(\theta(t))$ is the Jacobian matrix and defined as $J(\theta(t)) = \partial f(\theta(t))/\partial\theta(t)$.

2.2. QP subproblems of left and right manipulators

Based on the above fundamental kinematics equations, the kinematics equations of the left and the right manipulators can be obtained as follows:

$$r_R(t) = f_R(\theta_R(t)) \tag{4}$$

$$r_L(t) = f_L(\theta_L(t)) \tag{5}$$

where $r_L(t) \in R^m$ and $r_R(t) \in R^m$ denote the end-effector vectors of left and right redundant manipulators respectively. $\theta_L(t) \in R^n$ and $\theta_R(t) \in R^n$ denote joint vectors of left and right redundant manipulators respectively. The definitions of $f_L(\cdot)$ and $f_R(\cdot)$ are the same as Eq. (1). For the PUMA560, due to the structure of the given task, the dimensionality of joint space is 6 and the dimensionality of task space is 3 so that $n = 6$ and $m = 3$. Similarly, the rest of the classic formulas for the left and the right redundant manipulators can be written as

$$J_L(\theta_L)\dot{\theta} = \dot{r}_L \tag{6}$$

$$J_R(\theta_R)\dot{\theta} = \dot{r}_R \tag{7}$$

https://doi.org/10.1017/S026357471900119X Published online by Cambridge University Press

$$J_L(\theta_L)\ddot{\theta}_L = \ddot{r}_{La} = \ddot{r}_L - \dot{J}_L(\theta_L)\dot{\theta}_L \tag{8}$$

$$J_R(\theta_R)\ddot{\theta}_R = \ddot{r}_{Ra} = \ddot{r}_R - \dot{J}_R(\theta_R)\dot{\theta}_R \tag{9}$$

where $J_L(\theta_L) \in R^{m\times n}$ and $J_R(\theta_R) \in R^{m\times n}$ are the Jacobian matrixes of the left and right manipulators respectively and defined as $J_L(\theta_L) = \partial f_L(\theta_L)/\partial\theta_L$ and $J_R(\theta_R) = \partial f_R(\theta_R)/\partial\theta_R$, respectively. $\dot{r}_L \in R^m$ and $\dot{r}_R \in R^m$ denote the end-effector velocity vectors of the left and right redundant manipulators, respectively. Besides, $\ddot{r}_L \in R^m$ and $\ddot{r}_R \in R^m$ are the end-effector acceleration vectors of the left and right redundant manipulators, respectively. $\dot{J}_L(\theta_L) \in R^{m\times n}$ and $\dot{J}_R(\theta_R) \in R^{m\times n}$ are the time derivative of Jacobian matrix of the left and right redundant manipulators. Note that $J_L(\theta_L)$, $J_R(\theta_R)$, $\dot{J}_L(\theta_L)$, and $\dot{J}_R(\theta_R)$ can be abbreviated to J_L, J_R, $\dot{J}_L$, and $\dot{J}_R$.

In order to control the manipulators at the joint-acceleration-level with consideration of joint-angle drift, the ALTC-OMP scheme is proposed, which integrates the optimization criteria of the MAN, RMP, and INAM. The acceleration-level QP problem with tri-criteria optimization scheme can be designed as:

$$\begin{aligned}\text{min. } \gamma_{L/R}\|\ddot{\theta}_{L/R}\|_2^2/2 + \delta_{L/R}\|\ddot{\theta}_{L/R} + C_{L/R}\|_2^2/2 + \\ (1-\gamma_{L/R}-\delta_{L/R})\|\ddot{\theta}_{L/R}\|_\infty^2/2\end{aligned} \tag{10}$$

where $\|\cdot\|_2$ and $\|\cdot\|_\infty$ respectively denote the two-norm and an infinite norm of a vector. The design parameters $\gamma_{L/R}$, $\delta_{L/R}$, and $(1-\gamma_{L/R}-\delta_{L/R})$ are weighting parameters which are used respectively to adjust the weights of MAN, RMP, and INAM. The design parameters should be satisfied simultaneously $\gamma_{L/R} \in (0, 1)$, $\delta_{L/R} \in (0, 1)$, and $((\gamma_{L/R}+\delta_{L/R}) \in (0, 1))$. In general, when the factor $\delta_{L/R}$ is closer to 1, the proposed ALTC-OMP scheme places emphasis on $\|\ddot{\theta}_{L/R} + C\|_2^2/2$. Similarly, when the factor $\gamma_{L/R}$ or $(1-\gamma_{L/R}-\delta_{L/R})$ is closer to 1, the proposed ALTC-OMP scheme places emphasis on $\|\ddot{\theta}_{L/R}\|_2^2/2$ or $\|\ddot{\theta}_{L/R}\|_\infty^2/2$. In a word, the design parameters $\gamma_{L/R}$ and $\delta_{L/R}$ are adjusted as need of the tracking task. $C_{L/R}$ is defined as $(\alpha+\beta)\dot{\theta}_{L/R} + \alpha\beta[\theta_{L/R} - \theta_{L/R}(0)]$, where α and β are positive design parameters. Theoretically, the design parameters α and β should be as larger as possible. In the actual application process, the parameters should be gradually increased from small to large until the actual demand is met. However, considering the physical conditions such as joint-angle limits of redundant manipulators and the computational performance, the design parameters α and β are set as $\alpha = \beta$=5 which can meet the accuracy requirement without causing too much burden on the computers and redundant arms.

In engineering applications, almost all manipulators have physical limits, so it is more practical and useful to consider joint-angle limits, joint-velocity limits, and joint-acceleration limits in the scheme formulation. For the left redundant manipulator, the proposed ALTC-OMP scheme can be written as:

$$\begin{aligned}\text{min. } \gamma_L\|\ddot{\theta}_L\|_2^2/2 + \delta_L\|\ddot{\theta}_L + C_L\|_2^2/2 + \\ (1-\gamma_L-\delta_L)\|\ddot{\theta}_L\|_\infty^2/2\end{aligned} \tag{11}$$

$$\text{s.t. } J_L(\theta_L)\ddot{\theta}_L = \ddot{r}_L - \dot{J}_L(\theta_L)\dot{\theta}_L \tag{12}$$

$$\theta_L^- \leqslant \theta_L \leqslant \theta_L^+ \tag{13}$$

$$\dot{\theta}_L^- \leqslant \dot{\theta}_L \leqslant \dot{\theta}_L^+ \tag{14}$$

$$\ddot{\theta}_L^- \leqslant \ddot{\theta}_L \leqslant \ddot{\theta}_L^+ \tag{15}$$

with $C_L = (\alpha+\beta)\dot{\theta}_L + \alpha\beta[\theta_L - \theta_L(0)]$

where γ_L, δ_L, J_L, and $\dot{J}_L$ are defined the same as before. θ_L^- and θ_L^+ denote the lower and upper limits of the joint-angle vectors. $\dot{\theta}_L^-$ and $\dot{\theta}_L^+$ denote the lower and upper limits of the joint-angle velocity vectors. $\ddot{\theta}_L^-$ and $\ddot{\theta}_L^+$ denote the lower and upper limits of the joint-angle acceleration vectors. Equation (12) is the forward kinematics equation of the left robot manipulator of dual manipulators. $\theta_L(0)$ denotes the initial value of the joint angle vector $\theta_L(t)$.

Similarly, ALTC-OMP scheme of the right redundant manipulator is designed as:

$$\begin{aligned}\text{min. } \gamma_R\|\ddot{\theta}_R\|_2^2/2 + \delta_R\|\ddot{\theta}_R + C_R\|_2^2/2 + \\ (1-\gamma_R-\delta_R)\|\ddot{\theta}_R\|_\infty^2/2\end{aligned} \tag{16}$$

https://doi.org/10.1017/S026357471900119X Published online by Cambridge University Press

$$\text{s.t. } J_R(\theta_R)\ddot{\theta}_R = \ddot{r}_R - \dot{J}_R(\theta_R)\dot{\theta}_R \tag{17}$$
$$\theta_R^- \leqslant \theta_R \leqslant \theta_R^+ \tag{18}$$
$$\dot{\theta}_R^- \leqslant \dot{\theta}_R \leqslant \dot{\theta}_R^+ \tag{19}$$
$$\ddot{\theta}_R^- \leqslant \ddot{\theta}_R \leqslant \ddot{\theta}_R^+ \tag{20}$$

with $C_R = (\alpha + \beta)\dot{\theta}_R + \alpha\beta[\theta_R - \theta_R(0)]$
where γ_R, δ_R, J_R, $\dot{J}_R$, θ_R^- and θ_R^+, $\dot{\theta}_R^-$ and $\dot{\theta}_R^+$, $\ddot{\theta}_R^-$ and $\ddot{\theta}_R^+$, and $\theta_R(0)$ are defined the same as before.

3. Reformulation, Unification, and Solution of QP

In this section, QP problem of the redundant manipulator is solved at the acceleration-level. First of all, QP problems Eqs. (11)–(15) and Eqs. (16)–(20) are reformulated into two concise QP problems; then the two reformulated QP problems are unified into one standard QP problem. Finally, the unified QP problem is solved by the S-LVI-PDNN solver.

3.1. Reformulation

In this subsection, the Eqs. (11)–(20) are reformulated into two concise QP problems for the convenience of expression.

1. Conversion of MAN criterion and RMP criterion: through mathematical manipulation, the first and second terms of Eq. (11) can be rewritten equivalently as:

$$\gamma_L\ddot{\theta}_L^T I\ddot{\theta}_L/2 \ \textit{ and } \ \delta_L(\ddot{\theta}_L^T I\ddot{\theta}_L + \Lambda_L\ddot{\theta}_L)/2 \tag{21}$$

   where the superscript T denotes the transpose of a vector (or a matrix), $I \in R^{n+m}$ denotes an identity matrix, and $\Lambda_L = 2(\alpha + \beta)\dot{\theta}_L + 2\alpha\beta[\theta_L - \theta_L(0)]$.
2. Conversion of INAM criterion: By defining $g_L = \|\ddot{\theta}_L\|_\infty$, the INAM criterion $(1 - \gamma_L - \delta_L)\|\ddot{\theta}_L\|_\infty^2/2$ in the third terms (11) of the redundant manipulator can be rewritten equivalently as:

$$\text{min.} \qquad (1 - \gamma_L - \delta_L)g_L^2/2 \tag{22}$$
$$\text{s.t.} \quad \begin{bmatrix} I & -I_v \\ -I & -I_v \end{bmatrix} \begin{bmatrix} \ddot{\theta}_L \\ g_L \end{bmatrix} \leqslant \begin{bmatrix} 0 \\ 0 \end{bmatrix} \tag{23}$$

   where I_v is a vector whose all elements are ones (i.e., $I_v = [1, 1, ..., 1]^T \in R^{n+m}$).
3. Conversion of joint limits: because the Eqs. (11)–(20) are solved at the acceleration-level, joint physical limit (13) and (14) should be transformed into the formulations about $\ddot{\theta}_L$. First, the lower limit and the upper limit (13) can be rewritten in terms of $\ddot{\theta}_L$ by using the following conversion:

$$\ddot{\theta}_L \geq \kappa_\alpha(\lambda\theta_L^- - \theta_L) \tag{24}$$
$$\ddot{\theta}_L \leq \kappa_\alpha(\lambda\theta_L^+ - \theta_L) \tag{25}$$

   Considering the inertia movement, design parameter $\lambda \in (0, 1)$ is used to define the critical regions $[\theta_L^-, \lambda\theta_L^-]$ and $[\lambda\theta_L^+, \theta_L^+]$ which is derived from the inertial movement during deceleration. When the joints enter such a critical region a deceleration will occur. The design parameter $\kappa_\alpha > 0$ is used to determine the magnitude of such a deceleration. Similarly, the avoidance of the velocity limits $\dot{\theta}_L^\pm$ in (14) can be converted as:

$$\kappa_\beta(\dot{\theta}_L^- - \dot{\theta}_L) \leq \ddot{\theta}_L \leq \kappa_\beta(\dot{\theta}_L^+ - \dot{\theta}_L) \tag{26}$$

   Equation (26) guarantees that the joint-acceleration gradually changes the direction when the joint-velocity approaches their limits. The intensity coefficients $\kappa_\alpha > 0$ and $\kappa_\beta > 0$ determine the deceleration magnitude when the robot joints enter the aforementioned critical area. Generally speaking, the intensity coefficients $\kappa_\alpha > 0$ and $\kappa_\beta > 0$ should be chosen such that the feasible region of $\ddot{\theta}$ converted by joint-angle and joint-velocity limits is larger than the original one made by the joint-acceleration (15). In the simulations, the design parameters are set as $\kappa_\alpha = \kappa_\beta$ =20. Through conversing bound constraints (13) and (14) into (24)–(26) respectively, the bound constraints about θ_L and $\dot{\theta}_L$ can be expressed by the bound constraints about $\ddot{\theta}_L$ with a set of scaling

https://doi.org/10.1017/S026357471900119X Published online by Cambridge University Press

parameters. Thus the bound constraints (13)–(15) can be combined into a unified bound constraint whose lower limit and upper limit can be expressed as:

$$\zeta_L^- = \max\{\kappa_\alpha(\lambda\theta_L^- - \theta_L), \kappa_\beta(\dot{\theta}_L^- - \dot{\theta}_L), \ddot{\theta}_L^-\} \tag{27}$$

$$\zeta_L^+ = \min\{\kappa_\alpha(\lambda\theta_L^+ - \theta_L), \kappa_\beta(\dot{\theta}_L^+ - \dot{\theta}_L), \ddot{\theta}_L^+\} \tag{28}$$

4. Scheme reformulation: By defining the augmented variable vector $x_L = [\ddot{\theta}_L^T, g_L]^T \in R^{n+1}$, the presented ALTC-OMP scheme can be reformulated into a standard QP as follows:

$$\text{min. } x_L^T W_L x_L/2 + p_L^T x_L \tag{29}$$

$$\text{s.t. } B_L x_L = b_L \tag{30}$$

$$E_L x_L \le d_L \tag{31}$$

$$x_L^- \le x_L \le x_L^+ \tag{32}$$

$$W_L = \begin{bmatrix} (\gamma_L + \delta_L)I & 0 \\ 0 & (1 - \gamma_L - \delta_L) \end{bmatrix} \in R^{(n+1)\times(n+1)},$$

$$p_L = \begin{bmatrix} \delta_L(\mu + \nu)\dot{\theta}_L + \delta_L\mu\nu(\theta_L - \theta_L(0)) \\ 0 \end{bmatrix}^T \in R^{(n+1)}, B_L = \begin{bmatrix} J_L & 0 \end{bmatrix} \in R^{m\times(n+1)}$$

$$b_L = (\ddot{r}_L - \dot{J}_L(\theta)\dot{\theta}_L) \in R^m,$$

$$E_L = \begin{bmatrix} I & -I_v \\ -I & -I_v \end{bmatrix} \in R^{2n\times(n+1)}, d_L = 0 \in R^{2n}, x_L^- = \begin{bmatrix} \zeta_L^- \\ 0 \end{bmatrix} \in R^{n+1}, x_L^+ = \begin{bmatrix} \zeta_L^+ \\ \varpi \end{bmatrix} \in R^{n+1}$$

where ϖ is a large constant, which is used to replace $+\infty$ numerically.
Similarly, the QP reformulation of the right redundant manipulator is the same as that of the left redundant manipulator, which can be finally presented as:

$$\text{min. } x_R^T W_R x_R/2 + p_R^T x_R \tag{33}$$

$$\text{s.t. } B_R x_R = b_R \tag{34}$$

$$E_R x_R \le d_R \tag{35}$$

$$x_R^- \le x_R \le x_R^+ \tag{36}$$

where the definitions of W_R, p_R, B_R, b_R, E_R, d_R, x_R^-, and x_R^+ are similar to those of the left robot manipulator.

3.2. Unification

According to the Eqs. (29)–(32) and (33)–(36), the dual redundant manipulators of the proposed scheme can be unified into one standard QP, that is,

$$\text{min. } x^T C x/2 + \omega^T z \tag{37}$$

$$\text{s.t. } Qx = h \tag{38}$$

$$Az \le e \tag{39}$$

$$x^- \le x \le x^+ \tag{40}$$

$$C = \begin{bmatrix} W_L & 0 \\ 0 & W_R \end{bmatrix} \in R^{2(n+1)\times(n+1)}, \quad x = \begin{bmatrix} x_L \\ x_R \end{bmatrix} \in R^{2(n+1)}, \quad Q = \begin{bmatrix} B_L & 0 \\ 0 & B_R \end{bmatrix} \in R^{2m\times(n+1)},$$

$$\omega = \begin{bmatrix} p_L \\ p_R \end{bmatrix} \in R^{2(n+1)}, \quad h = \begin{bmatrix} b_L \\ b_R \end{bmatrix} = \begin{bmatrix} \ddot{r}_L - \dot{J}_L\dot{\theta}_L \\ \ddot{r}_R - \dot{J}_R\dot{\theta}_R \end{bmatrix} \in R^{2m}, \quad A = \begin{bmatrix} E_L & 0 \\ 0 & E_R \end{bmatrix} \in R^{4n\times 2(n+1)},$$

$$e = 0 \in R^{4n}, \quad x^- = \begin{bmatrix} x_L^- \\ x_R^- \end{bmatrix} \in R^{2(n+1)}, \quad x^+ = \begin{bmatrix} x_L^+ \\ x_R^+ \end{bmatrix} \in R^{2(n+1)}$$

Owing to C is a positive definite matrix, the Eqs. (37)–(40) is strictly convex, which guarantee the uniqueness of solution to the QP problem.

https://doi.org/10.1017/S026357471900119X Published online by Cambridge University Press

3.3. Solution

It is worth pointing out that the proposed scheme ALTC-OMP and the corresponding QP problem (37)–(40) can be solved by S-LVI-PDNN solver.

First, QP problem (37)–(40) is converted to an LVI problem. That is to find a primal-dual equilibrium matrix $y^* \in \Omega$ and $\forall y \in \Omega := \{y | y^- \le y \le y^+\} \subset R^{2(3n+m+1)}$

$$(y - y^*)^T (My^* + g) \ge 0 \tag{41}$$

where the primal-dual decision variable vector y and its lower and upper bounds are defined as:

$$y = \begin{bmatrix} x \\ u \\ v \end{bmatrix}, y^- = \begin{bmatrix} x^- \\ -I_v \varpi \\ 0 \end{bmatrix}, y^+ = \begin{bmatrix} x^+ \\ I_v \varpi \\ I_v \varpi \end{bmatrix}$$

where dual decision vector $u \in R^{2m}$ and $v \in R^{4n}$ are defined for equality constraint (38) and inequality constraint (39) respectively. In addition, the augmented matrix M and vector q are defined as

$$M = \begin{bmatrix} C & -Q^T & A^T \\ Q & 0 & 0 \\ -A & 0 & 0 \end{bmatrix} \in R^{2(3n+m+1)\times 2(3n+m+1)}, \quad g = \begin{bmatrix} \omega \\ -h \\ e \end{bmatrix} \in R^{2(3n+m+1)}$$

Second, according to the refs. [53, 54], we know that the Eq. (41) is equivalent to a corresponding piecewise-linear equations:

$$P_\Omega(y - (My + g)) - y = 0 \tag{42}$$

where $P_\Omega(\cdot) : R^{2(3n+m+1)} \to \Omega$ and the ith element of $P_\Omega(y)$ is a projection operator and defined as:

$$\begin{cases} y_i^-, & if \quad y_i < y_i^-, \\ y_i, & if \quad y_i^- \le y_i \le y_i^+, \\ y_i^+, & if \quad y_i \ge y_i^+, \end{cases}$$

Third, according to our neural network design experience in refs. [53–55], based on the primal dual neural networks, the Eq. (42) can be further computed by the LVI-based primal dual neural networks (LVI-PDNN):

$$\dot{y} = \eta(I + M^T)(P_\Omega(y - (My + g)) - y) \tag{43}$$

Finally, in order to simplify the calculation and realization of real-time solver (43), the scaling matrix $(I + M^T)$ is eliminated from (43), and then the S-LVI-PDNN can be obtained as:

$$\dot{y} = \eta(P_\Omega(y - (My + g)) - y) \tag{44}$$

where positive parameter η is designed to adjust the convergence rate of neural network (44), which also affects the convergence rate of the position errors. Generally speaking, the larger parameter η is set, the faster convergence of the position errors is gotten, and the more consumed time for computer simulation is spent. Considering the performance of the computer and practical applications, parameter η is set as 10^7. Furthermore, we have the global exponential convergence of the presented S-LVI-PDNN when solving the QP problem (37)–(40) in real time.

4. Computer Simulations

In this section, computer simulations based on two PUMA560 redundant manipulators are performed to illustrate the advantages of the proposed ALTC-OMP scheme.

In the computer simulations, three different path-tracking examples, that is, an English letter "W," Chinese character "silk," and Chinese characters "one belt one road," are illustrated in this paper. The joint-angle, joint-angle, and joint-accelerator physical limits of the dual PUMA560 redundant manipulators used in the simulations are shown in Table I. Designed parameters are set as $\gamma = \gamma_L = \gamma_R$, $\delta = \delta_L = \delta_R$, $\kappa_\alpha = \kappa_\beta = 20$, $\alpha = 5$, $\beta = 5$, and $\lambda = 0.9$. Note that the S-LVI-PDNN solver is used to solve the QP problem (37)–(40) in order to control the PUMA560 redundant manipulators, and the design parameter η is set as 10^7 through the paper. In order to illustrate the advantages of ALTC-OMP scheme, the simulations of the MAN scheme (i.e., γ=1 and δ=0) and the MAN-INAM scheme

https://doi.org/10.1017/S026357471900119X Published online by Cambridge University Press

Table I. Joint-angle, joint-velocity, and joint-accelerate physical limited.

Joint	$\theta^{+}_{L/R}$**(rad)**	$\theta^{-}_{L/R}$**(rad)**	$\dot{\theta}^{+}_{L/R}$**(rad)**	$\dot{\theta}^{-}_{L/R}$**(rad)**	$\ddot{\theta}^{+}_{L/R}$**(rad)**	$\ddot{\theta}^{-}_{L/R}$**(rad)**
1	2.7751	−2.7751	1.5000	−1.5000	4.0000	−4.0000
2	0.7505	−3.1416	1.5000	−1.5000	4.0000	−4.0000
3	3.1416	−0.9058	1.5000	−1.5000	4.0000	−4.0000
4	2.9671	−1.9199	1.5000	−1.5000	4.0000	−4.0000
5	0.0349	−1.7453	1.5000	−1.5000	4.0000	−4.0000
6	3.1416	−3.1416	1.5000	−1.5000	4.0000	−4.0000

Table II. Joint-drift comparisons among the MAN, MAN-INAM, and ALTC-OMP at the acceleration-level when the end-effector of the dual Redundant manipulators tracking the English word "W" path motion planning.

Scheme	**Left joints**	**Left joint drifts**	**Right joints**	**Right joint drifts**
	$\theta_{L1}(4)-\theta_{L1}(0)$	1.984×10^{-1}	$\theta_{R1}(4)-\theta_{R1}(0)$	1.984×10^{-1}
	$\theta_{L2}(4)-\theta_{L2}(0)$	3.240×10^{-1}	$\theta_{R2}(4)-\theta_{R2}(0)$	3.24×10^{-1}
MAN scheme	$\theta_{L3}(4)-\theta_{L3}(0)$	-3.131×10^{-1}	$\theta_{R3}(4)-\theta_{R3}(0)$	-3.13×10^{-1}
	$\theta_{L4}(4)-\theta_{L4}(0)$	-2.882×10^{-1}	$\theta_{R4}(4)-\theta_{R4}(0)$	-5.66×10^{-1}
($\gamma=1, \delta=0$)	$\theta_{L5}(4)-\theta_{L5}(0)$	-5.662×10^{-1}	$\theta_{R5}(4)-\theta_{12}(0)$	-7.850×10^{-1}
	$\theta_{L6}(4)-\theta_{L6}(0)$	6.130×10^{-25}	$\theta_{R6}(4)-\theta_{R6}(0)$	1.56×10^{-29}
	$\theta_{L1}(4)-\theta_{L1}(0)$	6.112×10^{-1}	$\theta_{R1}(4)-\theta_{R1}(0)$	4.849×10^{-1}
	$\theta_{L2}(4)-\theta_{L2}(0)$	9.628×10^{-1}	$\theta_{R2}(4)-\theta_{R2}(0)$	3.986×10^{-1}
MAN-INAM scheme	$\theta_{L3}(4)-\theta_{L3}(0)$	-1.578×10^{-0}	$\theta_{R3}(4)-\theta_{R3}(0)$	-3.088×10^{-1}
	$\theta_{L4}(4)-\theta_{L4}(0)$	-1.063×10^{-1}	$\theta_{R4}(4)-\theta_{R4}(0)$	-8.220×10^{-1}
($\gamma=0.5, \delta=0$)	$\theta_{L5}(4)-\theta_{L5}(0)$	-7.851×10^{-1}	$\theta_{R5}(4)-\theta_{R5}(0)$	-7.804×10^{-1}
	$\theta_{L6}(4)-\theta_{L6}(0)$	-1.895×10^{-25}	$\theta_{R6}(4)-\theta_{R6}(0)$	4.2253×10^{-26}
	$\theta_{L1}(4)-\theta_{L1}(0)$	-2.06719×10^{-5}	$\theta_{R1}(4)-\theta_{R1}(0)$	-2.06719×10^{-5}
	$\theta_{L2}(4)-\theta_{L2}(0)$	7.075×10^{-3}	$\theta_{R2}(4)-\theta_{R2}(0)$	7.075×10^{-3}
ALTC-OMP scheme	$\theta_{L3}(4)-\theta_{L3}(0)$	-7.136×10^{-3}	$\theta_{R3}(4)-\theta_{R3}(0)$	-7.136×10^{-3}
	$\theta_{L4}(4)-\theta_{L4}(0)$	-6.726×10^{-5}	$\theta_{R4}(4)-\theta_{R4}(0)$	-6.726×10^{-5}
($\gamma=0.1, \delta=0.5$)	$\theta_{L5}(4)-\theta_{L5}(0)$	-9.908×10^{-3}	$\theta_{R5}(4)-\theta_{12}(0)$	-9.908×10^{-3}
	$\theta_{L6}(4)-\theta_{L6}(0)$	4.837×10^{-28}	$\theta_{R6}(4)-\theta_{R6}(0)$	8.584×10^{-35}

(i.e., γ=0.5 and δ=0) of tracking the path of English letter "W" are performed. Besides, the Chinese characters about "silk" and "one belt one road" path are performed only on ALTC-OMP scheme.

4.1. English letter "W" path-tracking examples

The PUMA560 end-effectors are expected to simultaneously and collaboratively track an English letter "W" path. The task duration $t=4\times T=4s$ (i.e., T = 1s) and the initial states $\theta_L(0)=[\pi/2, \pi/8, 0, \pi/3, -\pi/2, 0]^T$, $\theta_R(0)=[-\pi/2, \pi/8, 0, \pi/3, -\pi/2, 0]^T$. The corresponding simulation results are illustrated in Figs. 2–4 and Table II.

First, Figs. 2, 3, 4 respectively show the motion trajectories simulation results synthesized by MAN scheme without considered physical constant (i.e., Eqs. (37)–(39) with $\gamma=1$ and $\delta=0$), MAN-INAM scheme without considered physical constant (i.e., Eqs. (37)–(39) with $\gamma=0.5$ and $\delta=0$), ALTC-OMP scheme with considered the physical constant (i.e., Eqs. (37)–(40) with $\gamma=0.1$ and $\delta=0.5$). Table II shows the detailed joint-angle drift about MAN scheme, MAN-INAM scheme, and ALTC-OMP scheme, respectively.

As seen from Fig. 2(a), the path tracking task is completed, which can be verified from the end-effector position-error (i.e., $\varepsilon=f(\theta(t))-f(\theta(0))$ less than 5×10^{-3}(m)) in Fig. 2(b)–(c). However, through Fig. 2(a), we can see that the final state of joint-angle is far away from the initial state after finishing the task, which means that joint-angle drift phenomenon happens. Further validation can be seen in Fig. 2(d)–(e) and the first row in Table II. Figure 2 (d)–(e) represent the profile of joint angles during task operation, and the ideal state is the final state coinciding with the initial state after

https://doi.org/10.1017/S026357471900119X Published online by Cambridge University Press

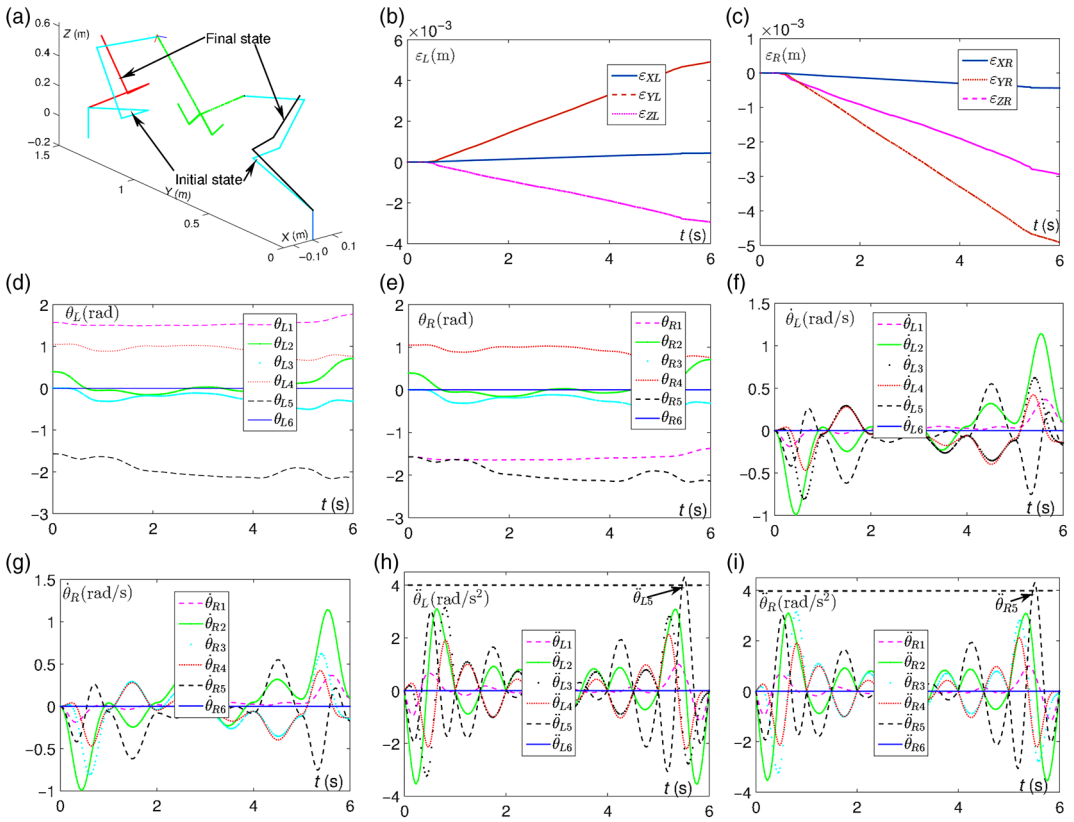

Fig. 2. Dual PUMA560 motion trajectories of an English letter "W" path synthesized by the MAN (with $\gamma = 1$ and $\delta = 0$). (a): End-effector trajectories of left and right redundant manipulators. (b) and (c): End-effector positioning-errors of left and right redundant manipulators. (d) and (e): Joint-angle profiles of left and right redundant manipulators. (f) and (g): Joint-velocity profiles of left and right redundant manipulators. (h) and (i): Joint-accelerator profiles of left and right redundant manipulators.

finishing the task. However, from Fig. 2(d)–(e), we see that the value of final state is far away from the initial state. Exact detailed actual drift of the joint-angle (i.e., $\theta(t) - \theta(0)$) can be seen from the first row in Table II, which are almost greater than -7.85×10^{-1}(rad) except θ_{6L} and θ_{6R}. That is to say, the joint-angle drift has happened in this simulation. Unfortunately, joint-angle drift can lead to accumulative errors, even damage to the redundant manipulator. Furthermore, comparing the curves in Fig. 2(f)–(g) and (h)–(i) with the data in Table I, it can be found that all the joint-velocities are kept within their joint limits, but the joint-acceleration exceeds its upper limit 4(rad/s^2) at about $t = 5.56$ (s), which may damage the redundant manipulators. In addition, as shown in Fig. 2 (f)–(g), the joint-velocity is not to be near zero after completion the task, which may hurt the people or damage the manipulator in the application of the redundant manipulator.

Second, Fig. 3 (a) shows the motion trajectories of dual PUMA560 redundant manipulators synthesized by the MAN-INAM scheme without considering the physical constrain ($\gamma = 0.5$ and $\delta = 0$). As shown in Fig. 3(b)–(c), comparing with MAN scheme, the MAN-INAM scheme can decrease position-errors between the initial state and final state (i.e., $\varepsilon = f(\theta(t)) - f(\theta(0))$ less than 4×10^{-4}(m)), and the joint-velocities and joint-acceleration are within the joint limits, respectively. However, from Fig. 3(a) and (d)–(e), we can see that the joint-angle drift phenomenon also happens. The exact actual drift of the joint-angle is shown in Table II about the MAN-INAM scheme (i.e., greater than -8.2×10^{-1}(rad) except θ_{6L} and θ_{6R}). Furthermore, the joint-velocity is not to be near zero after completing the task. The joint-velocity being not to zero at final terminal are unapplicable in practical applications.

Third, Fig. 4 shows the motion trajectory of dual PUMA560 redundant manipulators synthesized by the ALTC-OMP ($\gamma = 0.1$ and $\delta = 0.5$) scheme. Comparing with Figs. 2 (a) and 3 (a), we can see that the English letter "W" is tracked very well and the final joint state totally coincides with the initial state. The exact detailed joint-angle drifts can be seen from Table II about the ALTC-OMP scheme

https://doi.org/10.1017/S026357471900119X Published online by Cambridge University Press

Table III. Joint-drift-mean by ALTC-OMP scheme (i.e., $\gamma = 0.1$ or $\gamma = 0.3$ with different δ) at the acceleration-level when the end-effector of the dual Redundant manipulators tracking the English word "W" path motion planning.

γ	δ	$\lvert\theta(t) - \theta(0)\rvert$(rad)	Mean	γ	δ	$\lvert\theta(t) - \theta(0)\rvert$(rad)	Mean
	0.3	$\lvert\theta(4) - \theta(0)\rvert \times 10^{-2}$ (rad)	1.161		0.3	$\lvert\theta(4) - \theta(0)\rvert \times 10^{-3}$ (rad)	9.268
$\gamma = 0.1$	0.5	$\lvert\theta(4) - \theta(0)\rvert \times 10^{-3}$ (rad)	7.502	$\gamma = 0.3$	0.5	$\lvert\theta(4) - \theta(0)\rvert \times 10^{-3}$ (rad)	4.140
	0.6	$\lvert\theta(4) - \theta(0)\rvert \times 10^{-3}$ (rad)	4.618		0.6	$\lvert\theta(4) - \theta(0)\rvert \times 10^{-3}$ (rad)	2.308

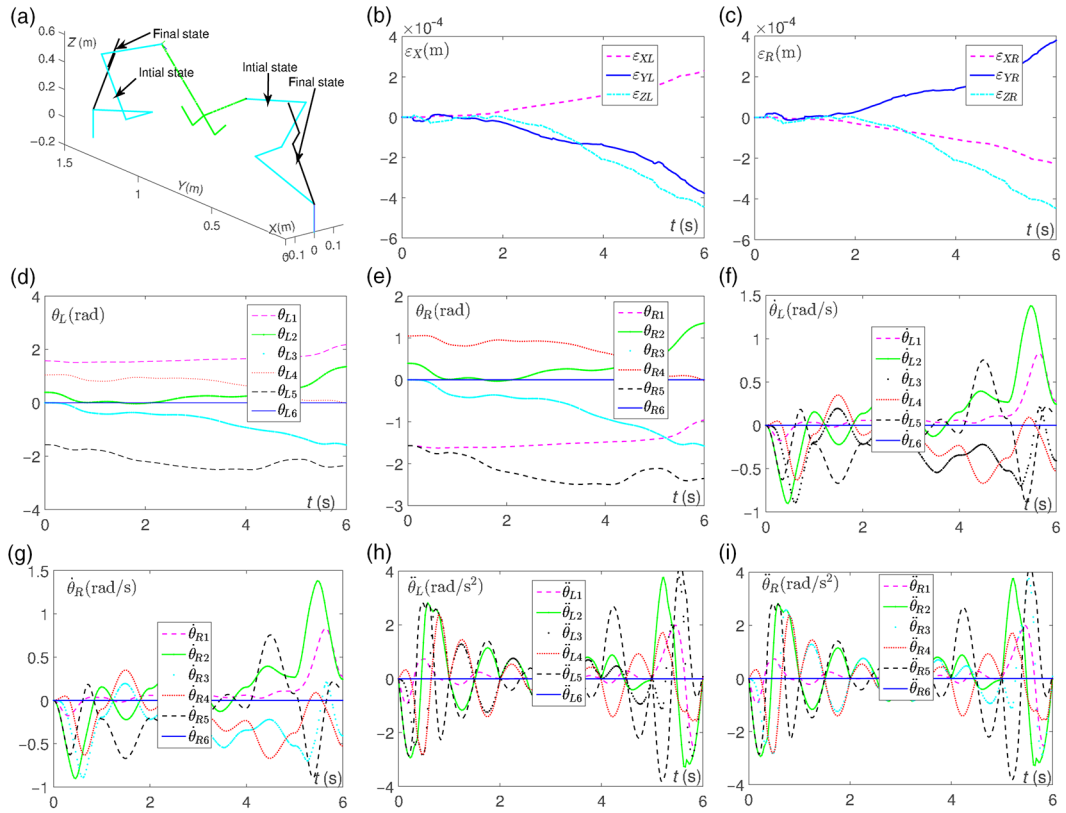

Fig. 3. Dual PUMA560 motion trajectories of an English letter "W" path synthesized by the MAN-INAM (with $\gamma = 0.5$ and $\delta = 0$). (a): End-effector trajectories of left and right redundant manipulators. (b) and (c): End-effector positioning-errors of left and right redundant manipulators. (d) and (e): Joint-angle profiles of left and right redundant manipulators. (f) and (g): Joint-velocity profiles of left and right redundant manipulators. (h) and (i): Joint-accelerator profiles of left and right redundant manipulators.

which are almost less than -7.0×10^{-3}(rad). In Table II, comparing with MAN scheme (joint-angle drifts are almost -7.85×10^{-1}(rad)) and MAN-INAM scheme (joint-angle drifts are less than -8.2×10^{-1}(rad)), the ALTC-OMP scheme joint-angle drifts are almost 7.075×10^{-3}(rad) which indicates that the joint-angle drift problem is solved well by the proposed ALTC-OMP scheme. This is because the RMP is considered in the proposed ALTC-OMP scheme. The proposed ALTC-OMP scheme can adjust the weights of the MAN, INAM, and RMP through readjusting the parameters γ and δ. Generally speaking , the designed parameter δ determines the RMP in the proposed ALTC-OMP scheme. Theoretically, when the designed parameter δ is determined, the designed parameter γ could be set close to 1 if small acceleration energy is of main concern, whereas the designed parameter γ could be set close to 0 if small joint-acceleration amplitude is of primary concern. The detailed values of the joint-angle drifts mean (i.e., the $\gamma = 0.1$ or $\gamma = 0.3$ with different δ) are shown in Table III. Figure 4 (f)–(g), (h)–(i) respectively show the joint-velocities and joint-acceleration of the dual redundant manipulators, which show that the joint-velocities and the joint-accelerations are within their joint limits, respectively. In addition, the joint-velocities and the joint-accelerations are near to zero when the dual redundant manipulators have finished the path-tracking task.

https://doi.org/10.1017/S026357471900119X Published online by Cambridge University Press

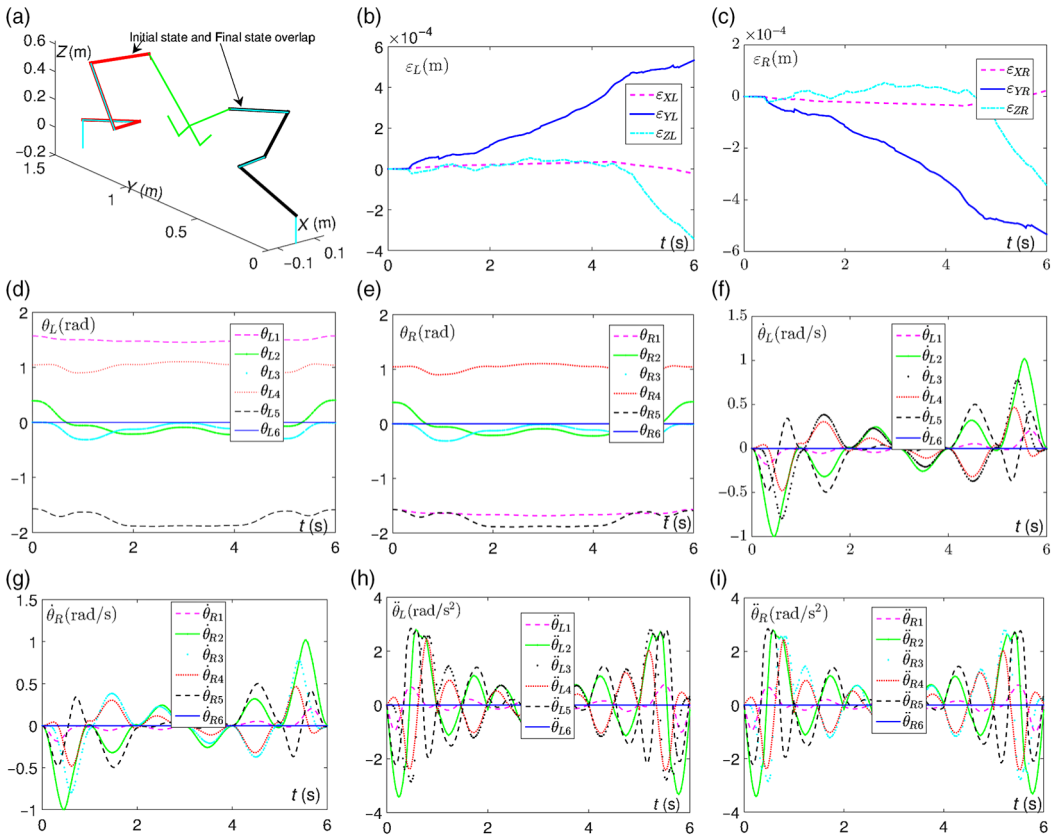

Fig. 4. Dual PUMA560 motion trajectories of a English letter "W" path synthesized by the MAN-RMP-INAM (with $\gamma = 0.1$ and $\delta = 0.5$). (a): End-effector trajectories of left and right redundant manipulators. (b) and (c): End-effector positioning-errors of left and right redundant manipulators. (d) and (e): Joint-angle profiles of left and right redundant manipulators. (f) and (g): Joint-velocity profiles of left and right redundant manipulators. (h) and (i): Joint-accelerator profiles of left and right redundant manipulators.

In summary, the difference among Figs. 2, 3, and 4 can be summarized as follows:

- It can be seen from Figs. 2 (b)–(c) and 3 (b)–(c) that the INAM-MAN scheme can reduce the position-error compared to the MAN scheme. From Figs. 2 (f)–(i) and 3 (f)–(i), the joint-velocity and joint-accelerator in the MAN-INAM scheme are within their physical limits compared to the MAN scheme.
- From Figs. 2 (a), 3(a), and 4 (a), the ALTC-OMP scheme can reduce joint-velocity drift problem in the task duration. From Fig. 4 (f)–(i), the joint-velocity and joint-accelerator in the ALTC-OMP scheme are within their physical limits and the value of the joint-velocity and joint-accelerator are near to zero at the last moment of execution.
- From Figs. 2 (d)–(e), 3(d)–(e), and 4 (d)–(e), the final value of joint-angle in VLTC-OMP scheme returns its initial value after finishing the task. However, the final value and the initial value of the joint-angle in the MAN and MAN-INAM are quite different.

4.2. Complex Chinese character path-tracking (i.e., named "silk" and "one belt one road")

In order to further illustrate the advantages of the proposed ALTC-OMP scheme, another two-path tracking (i.e., Chinese character (named "silk" and "one belt one road") path) is applied as the end-effector tracking tasks of the PUNA560 simultaneously and collaboratively. The motion-task duration $t = 15 \times T = 15\text{s}(i.e., T = 1\text{s})$ and $t = 40 \times T = 40\text{s}(i.e., T = 1\text{s})$ respectively. The initial states are $\theta_L(0) = [\pi/2, \pi/8, 0, \pi/3, -\pi/2, 0]^T$ and $\theta_R(0) = [-\pi/2, \pi/8, 0, \pi/3, -\pi/2, 0]^T$. The corresponding simulation results are illustrated in Figs. 5 and 6.

Figures 5 (a) and 6 (a) show the tracking result of the Chinese characters, from which we can see that the initial state of the joint-angle coincides with their finial state, which means that the two

https://doi.org/10.1017/S026357471900119X Published online by Cambridge University Press

Table IV. Joint-angle (RAD) drift by ALTC-OMP scheme at the acceleration-level when the end-effector of the dual redundant manipulators tracking the Chinese characters "silk" and "one belt one road" path.

Scheme	**Joints**	**Joint drifts**	**Joints**	**Joint drifts**
Chinese character "Silk" path ($\gamma = 0.1$, $\delta = 0.5$)	$\theta_{L1}(15) - \theta_{L1}(0)$	1.256×10^{-3}	$\theta_{R1}(15) - \theta_{R1}(0)$	9.765×10^{-4}
	$\theta_{L2}(15) - \theta_{L2}(0)$	1.034×10^{-2}	$\theta_{R2}(15) - \theta_{R2}(0)$	9.862×10^{-3}
	$\theta_{L3}(15) - \theta_{L3}(0)$	-2.332×10^{-3}	$\theta_{R3}(15) - \theta_{R3}(0)$	-3.7480×10^{-3}
	$\theta_{L4}(15) - \theta_{L4}(0)$	-1.088×10^{-5}	$\theta_{R4}(15) - \theta_{R4}(0)$	-2.016×10^{-3}
	$\theta_{L5}(15) - \theta_{L5}(0)$	-9.9204×10^{-3}	$\theta_{R5}(15) - \theta_{R5}(0)$	-9.342×10^{-3}
	$\theta_{L6}(15) - \theta_{L6}(0)$	-1.931×10^{-64}	$\theta_{R6}(15) - \theta_{R6}(0)$	1.606×10^{-34}
Chinese character "one belt one road" path ($\gamma = 0.1$, $\delta = 0.5$)	$\theta_{L1}(40) - \theta_{L1}(0)$	-3.958×10^{-5}	$\theta_{R1}(40) - \theta_{R1}(0)$	-6.784×10^{-4}
	$\theta_{L2}(40) - \theta_{L2}(0)$	-1.540×10^{-5}	$\theta_{R2}(40) - \theta_{R2}(0)$	-7.481×10^{-4}
	$\theta_{L3}(40) - \theta_{L3}(0)$	-4.367×10^{-5}	$\theta_{R3}(40) - \theta_{R3}(0)$	2.305×10^{-3}
	$\theta_{L4}(40) - \theta_{L4}(0)$	1.325×10^{-4}	$\theta_{R4}(40) - \theta_{R4}(0)$	2.852×10^{-3}
	$\theta_{L5}(40) - \theta_{L5}(0)$	8.591×10^{-5}	$\theta_{R5}(40) - \theta_{R5}(0)$	-1.111×10^{-2}
	$\theta_{L6}(40) - \theta_{L6}(0)$	2.072×10^{-172}	$\theta_{R6}(40) - \theta_{R6}(0)$	3.325×10^{-85}

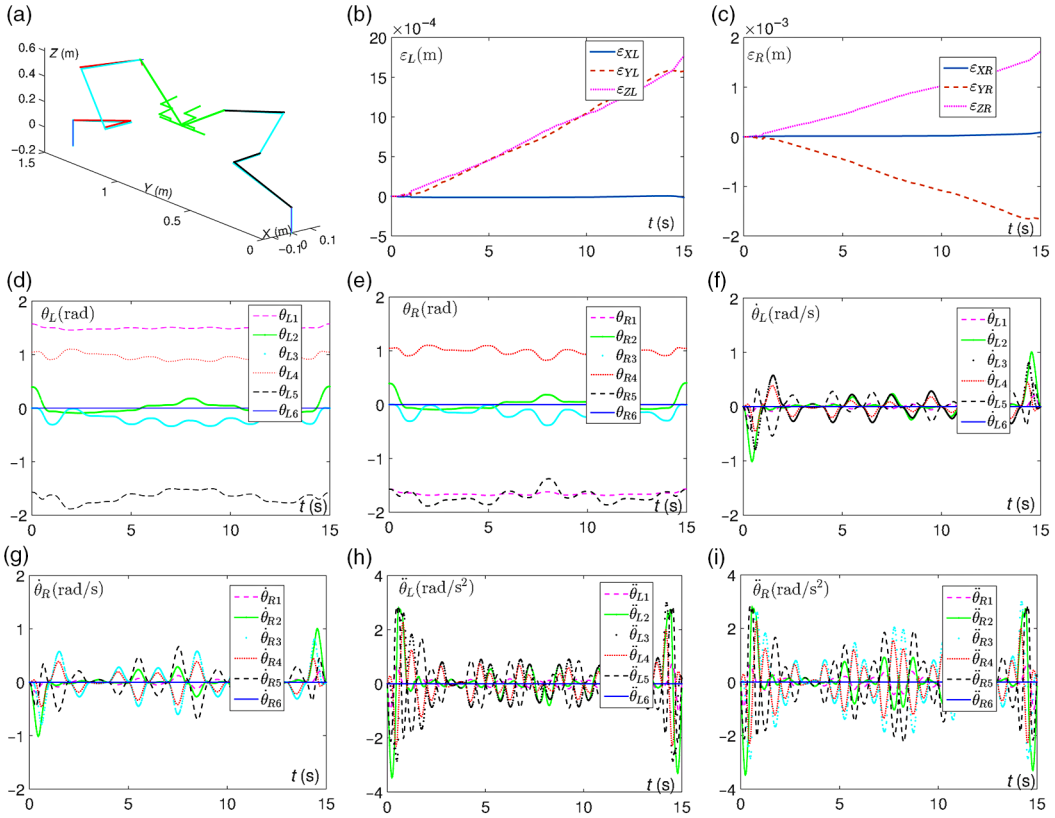

Fig. 5. Dual PUMA560 motion trajectories of Chinese character "silk" path synthesized by the ALTC-OMP (with $\gamma = 0.1$ and $\delta = 0.5$). (a): End-effector trajectories of left and right redundant manipulators. (b) and (c): End-effector positioning-errors of left and right redundant manipulators. (d) and (e): Joint-angle profiles of left and right redundant manipulators. (f) and (g): Joint-velocity profiles of left and right redundant manipulators. (h) and (i): Joint-accelerator profiles of left and right redundant manipulators.

complex path tracking is completed well and the joint-angle drift phenomenon is remedied well in this tracking simulation. The joint-angle drift errors of the two-path in Table IV (i.e., Chinese character (named "silk" and "one belt one road") path) are respectively less than 9.8×10^{-3}(rad) except θ_{L2} and 2.8×10^{-3}(rad) except θ_{R5}, which means that the proposed ALTC-OMP scheme can remedy joint-angle drift on complex path tracking. Figures 5 (b)–(c), (d)–(e), (f)–(j), (h)–(i) and 6 (b)–(c), (d)–(e), (f)–(j), (h)–(i) show position-errors, joint-angle profiles, joint-velocities profiles,

https://doi.org/10.1017/S026357471900119X Published online by Cambridge University Press

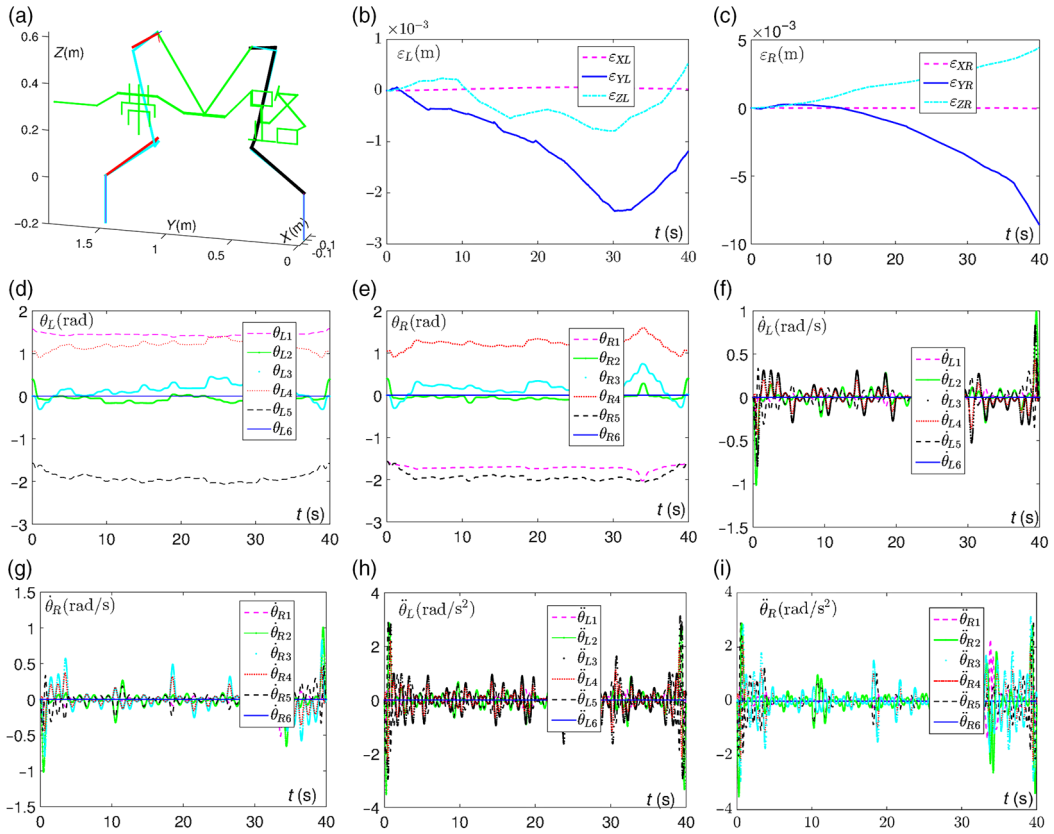

Fig. 6. Dual PUMA560 motion trajectories of Chinese characters "one belt one road" path synthesized by the ALTC-OMP (with $\gamma = 0.1$ and $\delta = 0.5$). (a): End-effector trajectories of left and right redundant manipulators. (b) and (c): End-effector positioning-errors of left and right redundant manipulators. (d) and (e): Joint-angle profiles of left and right redundant manipulators. (f) and (g): Joint-velocity profiles of left and right redundant manipulators. (h) and (i): Joint-accelerator profiles of left and right redundant manipulators.

and joint-acceleration profiles of the dual redundant manipulators, respectively. The end-effector position-errors about the two-path tracking are shown in Figs. 5 (b)–(c) and 6 (b)–(c), respectively. The position-errors are less than 4×10^{-3}(m). From Figs. 5 (d)–(e) and 6 (d)–(e), the θ_L and θ_R go back to their initial state. As seen further from Figs. 5 (f)–(j), (h)–(i) and 6 (f)–(j), (h)–(i), the $\dot{\theta}_L$ and $\dot{\theta}_R$, $\ddot{\theta}_L$ and $\ddot{\theta}_R$ approach to zero at the final terminal. The effectiveness of the ALTC-OMP scheme at acceleration-level subject to joint-angle limits, joint-velocity limits, and joint-acceleration limits is thus demonstrated.

5. Conclusions

In this paper, an ALTC-OMP integrating MAN, RMP, and INAM via weighting factor has proposed and investigated for complex motion planning and coordination control of dual redundant manipulators at acceleration-level. This scheme can not only remedy the joint-angle drift problem arising in dual redundant manipulators at acceleration-level, but also avoid the physical limits. Besides, the proposed scheme can guarantee the final joint-velocities and joint-acceleration near to zero of the manipulators. In addition, the proposed scheme is combined by two subschemes, and then two subschemes are reformulated as two QP problems (29)–(32) and (33)–(36), respectively. The two QP problems have been unified into one standard QP problem (37)–(40) and solved by the S-LVI-PDNN solver at the acceleration-level. The result of the simulation based on the dual PUMA560 redundant manipulators has demonstrated the effectiveness and feasibility of the proposed ALTC-OMP scheme on resolving the joint-angle drift of dual redundant manipulators. The future work is to apply such an ALTC-OMP scheme to practical industrial automation factories.

https://doi.org/10.1017/S026357471900119X Published online by Cambridge University Press

Acknowledgments
This research was supported by Science and Technology Plan of Guangzhou City (201903010063), Promotion and Innovation Plan of the Department of Agriculture and Rural Affairs of Guangdong Province (2018LM2164), National Key Research and Development Plan (2017YFD070100103), Key Science and Technology Plan of Guangdong Province (2017B010116003), the National Natural Science Foundation under Grants 61603142 and 61633010, the Guangdong Foundation for Distinguished Young Scholars under Grant 2017A030306009, the Guangdong Youth Talent Support Program of Scientific and Technological Innovation under Grant 2017TQ04X475, the Science and Technology Program of Guangzhou under Grant 201707010225, the Fundamental Research Funds for Central Universities under Grant x2zdD2182410, the National Key R and D Program of China under Grant 2017YFB1002505, the National Key Basic Research Program of China (973 Program) under Grant 2015CB351703, and the Guangdong Natural Science Foundation under Grant 2014A030312005.

References

1. C. Canali, N. Rahman, F. Chen, M. D'Imperio, D. Caldwell and F. Cannella, "Theoretical and kinematic solution of high reconfigurable grasping for industrial manufacturing," *Procedia Manuf.* **11**, 265–274 (2017).
2. R. Ul Islam, J. Iqbal, S. Manzoor, A. Khalid and S. Khan, "An Autonomous Image-Guided Robotic System Simulating Industrial Applications," *International Conference on System of Systems Engineering*, Genoa, Italy (2013) pp. 344–349.
3. W. Mustafa, N. Pugeault, A.G. Buch and N. Krüger, "Multi-view object instance recognition in an industrial context," *Robotica* **35**(2), 271–292 (2017).
4. Y. Yang, H. Chen, Y. Lou and W. Lin, "Remote Master-Slave Control of a 6D Manipulator for Cardiac Surgery Application," *IEEE International Conference on Robotics and Biomimetics*, Bali, Indonesia (2015) pp. 1799–1804.
5. J. Wang, Y. Yao and X. Kong, "A reconfigurable tri-prism mobile robot with eight modes," *Robotica*, **36**(10), 1454–1476 (2018).
6. F. Mazzini and S. Dubowsky, "An experimental validation of robotic tactile mapping in harsh environments such as deep sea oil well sites," *Springer Tracts Adv. Robot.* **79**, 557–570 (2014).
7. T. Zheng, D. T. Branson, E. Guglielmino, R. Kang, G. A. M. Cerda, M. Cianchetti, M. Follador, I. S. Godage and D. G. Caldwell, "Model validation of an octopus inspired continuum robotic arm for use in underwater environments," *J. Mech. Robot.* **5**(2), 021004 (2013).
8. H. M. La, "Automated robotic monitoring and inspection of steel structures and bridges," *Robotica*. **37**(5), 947–967 (2018).
9. K. Madhava Krishna, R. Alami and T. Simeon, "Safe proactive plans and their execution," *Robot. Auton. Syst.* **54**(3), 244–255 (2006).
10. M. H. Farzanehkaloorazi, M. T. Masouleh and S. Caro, "Collision-free workspace of parallel mechanisms based on an interval analysis approach," *Robotica* **35**(8), 1747–1760 (2018).
11. A. Khanpoor, A. K. Khalaji and S. A. A. Moosavian, "Modeling and control of an underactuated tractor-trailer wheeled mobile robot," *Robotica* **35**(12), 2297–2318 (2017).
12. Q. Xu and X. Sun, "Adaptive Operation-Space Control of Redundant Manipulators with Joint Limits Avoidance," *Tenth International Conference on Advanced Computational Intelligence*, Xiamen, China (2018) pp. 358–363.
13. H. Meng, M. Lin, S. Li, Z. Chen and D. Rong, "A Multi-Strategy Path Planner Based on Space Accessibility." *IEEE International Conference on Robotics and Biomimetics*, Macau SAR, China (2018) pp. 2154–2161.
14. R. M. Ferrús and M. D. Somonte, "Design in robotics based in the voice of the customer of household robots," *Robot. Auton. Syst.* **79**, 99–107 (2016).
15. A. K. Singh and K. Madhava Krishna, "Feasible acceleration count: A novel dynamic stability metric and its use in incremental motion planning on uneven terrain," *Robot. Auton. Syst.* **79**, 156–171 (2016).
16. S. Yahya, M. Moghavvemi and H. A. F. Mohamed, "Manipulability Constraint Locus for a Six Degrees of Freedom Redundant Planar Manipulator," *International Symposium on Computer, Consumer and Control*, Taichung, Taiwan (2012) pp. 290–293.
17. X. Ge and J. Jin, "Dynamics Analyze of a Dual-Arm Space Robot System Based on Kane's Method," *International Conference on Industrial Mechatronics and Automation*, Wuhan, China (2010) pp. 646–649.
18. M. Yazdani, R. S. Novin, M. T. Masouleh and M. B. Menhaj, "An Experimental Study on the Failure Tolerant Control of a Redundant Planar Serial Manipulator via Pseudo-Inverse Approach," *RSI International Conference on Robotics and Mechatronics*, Tehran, Iran (2015) pp. 365–370.
19. B. Cai and Y. Zhang, "Different-level redundancy-resolution and its equivalent relationship analysis for robot manipulators using gradient-descent and Zhang's neural-dynamic methods," *IEEE Trans. Ind. Electron.* **59**(8), 3146–3155 (2012).

20. D. Guo, X. Yan, L. Jin and H. Tan, "Ze in iZ1eD1 Manner for MKE Redundancy Resolution at Velocity and Acceleration levels," *International Conference on Systems and Informatics*, Shanghai, China (2014) pp. 45–50.
21. F. T. Cheng, T. H. Chen and Y. Y. Sun, "Resolving manipulator redundancy under inequality constraints," *IEEE Trans. Robot. Automat.* **10**(1), 65–71 (1994).
22. K. Chen, D. Guo, Z. Tan, Z. Yang and Y. Zhang, "Cyclic Motion Planning of Redundant Robot Arms: Simple Extension of Performance Index may not Work," *The Workshop on Intelligent Information Technology Applications*, NanChang, China (2009) pp. 635–639.
23. Y. Zhang and D. Guo, "Linear programming versus quadratic programming in robots' repetitive redundancy resolution: A chattering phenomenon investigation," *IEEE Conference on Industrial Electronics and Applications, ICIEA 2009*, Xi'an, China (2009) pp. 2822–2827 .
24. W. Xu, T. Liu and Y. Li, "Kinematics, dynamics, and control of a cable-driven hyper-redundant manipulator," *IEEE/ASME Trans. Mechatron.* **23**(4), 1693–1704 (2018).
25. S. Pedrammehr, B. Danaei, H. Abdi, M. T. Masouleh and S. Nahavandi, "Dynamic analysis of hexarot: Axis-symmetric parallel manipulator," *Robotica* **36**(2), 225–240 (2018).
26. H. B. Choi, S. Lee and J. Lee, "Minimum infinity-norm joint velocity solutions for singularity-robust inverse kinematics," *Int. J. Precis. Eng. Manufact.* **12**(3), 469–474 (2011).
27. Y. Zhang and K. Li, "Bi-criteria velocity minimization of robot manipulators using LVI-based primal-dual neural network and illustrated via puma560 robot arm," *Robotica* **28**(4), 525–537 (2010).
28. D. Guo and Y. Zhang, "Acceleration-level inequality-based man scheme for obstacle avoidance of redundant robot manipulators," *IEEE Trans. Indus. Electron.* **61**(12), 6903–6914 (2014).
29. Y. Zhang, J. Yin and B. Cai, "Infinity-norm acceleration minimization of robotic redundant manipulators using the LVI-based primal–dual neural network," *Robot. Comput. Integr. Manufact.* **25**(2), 358–365 (2009).
30. T. Wimbock and C. Ott, "Dual-arm manipulation," *Springer Tracts Adv. Robot.* **76**(10), 353–366 (2012).
31. Y. Zhang, B. Cai, L. Zhang and K. Li, "Bi-criteria velocity minimization of robot manipulators using a linear variational inequalities-based primal-dual neural network and puma560 example," *Adv. Robot.* **22**(13–14), 1479–1496 (2008).
32. D. Guo and Y. Zhang, "Different-level two-norm and infinity-norm minimization to remedy joint-torque instability/divergence for redundant robot manipulators," *Robot. Auton. Syst.* **60**(6), 874–888 (2012).
33. S. Liu and J. Wang, "A Dual Neural Network for Bi-Criteria Torque Optimization of Redundant Robot Manipulators," **In**: *Lecture Notes in Computer Science*, vol. 3316 (2004) pp. 1142–1147.
34. S. Liu and J. Wang, "Bi-Criteria Torque Optimization of Redundant Manipulators Based on a Simplified Dual Neural Network," *IEEE International Joint Conference on Neural Networks, IJCNN '05 Proceedings*, Montreal, Quebec, Canada, vol. 5 (2005) pp. 2796–2801.
35. B. Liao and W. Liu, "Pseudoinverse-type bi-criteria minimization scheme for redundancy resolution of robot manipulators," *Robotica* **33**(10), 2100–2113 (2015).
36. T. S. Wells, R. A. Maclachlan and C. N. Riviere, "Toward Hybrid Position/Force Control for an Active Handheld Micromanipulator," *IEEE International Conference on Robotics and Automation*, Hong Kong, China (2014) pp. 772–777.
37. T. Tsuji, J. Ohkuma and S. Sakaino, "Dynamic object manipulation considering contact condition of robot with tool," *IEEE Trans. Ind. Electron.* **63**(3), 1972–1980 (2016).
38. D. Nicolis, A. M. Zanchettin and P. Rocco, "Constraint-based and sensorless force control with an application to a lightweight dual-arm robot," *IEEE Robot. Automat. Lett.* **1**(1), 340–347 (2016).
39. M. Khansari, K. Kronander and A. Billard, "Modeling Robot Discrete Movements with State-Varying Stiffness and Damping: A Framework for Integrated Motion Generation and Impedance Control," *Robotics: Science and Systems*, Berkeley, California (2014).
40. L. I. H. Li, D. Wang, D. Yang, G. Zhang and L. I. Tiejun, "Research for dual-arm robot coordinated handling methods based on impedance control," *Mach. Tool Hydraul.* **45**(21), 64–97 (2017).
41. Z. Zhang and Y. Zhang, "Variable joint-velocity limits of redundant robot manipulators handled by quadratic programming," *IEEE/ASME Trans. Mechatron.* **18**(2), 674–686 (2013).
42. T. Asfour, P. Azad, F. Gyarfas and R. Dillmann, "Imitation learning of dual-arm manipulation tasks in humanoid robots," *Int. J. Human. Robot.* **5**(02), 183–202 (2006).
43. Y. C. Tsai and H. P. Huang, "Motion Planning of a Dual-Arm Mobile Robot in the Configuration-Time Space, *IEEE RSJ International Conference on Intelligent Robots and Systems*, St. Louis, USA (2009) pp. 2458–2463.
44. B. Cohen, S. Chitta and M. Likhachev, "Search-Based Planning for Dual-Arm Manipulation with Upright Orientation Constraints," *IEEE International Conference on Robotics and Automation*, St. Paul, Minnesota, USA (2012) pp. 3784–3790.
45. S. Peng, X. Ding, Y. Fan and K. Xu, "Motion planning and implementation for the self-recovery of an overturned multi-legged robot," *Robotica* **35**(5), 1107–1120 (2017).
46. M. Wang, J. Luo, J. Yuan and U. Walter, "Coordinated trajectory planning of dual-arm space robot using constrained particle swarm optimization," *Acta Astronaut.* **146**, 259–272 (2018).
47. Z. Huang, D. Chu, C. Wu and He Yi, "Path planning and cooperative control for automated vehicle platoon using hybrid automata," *IEEE Trans. Intell. Transport. Syst.* **20**(3), 1–16 (2018).
48. Y. Zhang, B. Cai, L. Zhang and K. Li, "Bi-criteria velocity minimization of robot manipulators using a linear variational inequalities-based primal-dual neural network and puma560 example," *Adv. Robot.* **22**(13–14), 1479–1496 (2008).

49. Y. Zhang, Y. Wang, D. Guo, X. Yu and L. Xiao, "Simultaneous repetitive motion planning of two redundant robot arms for acceleration-level cooperative manipulation," *Phys. Lett. Sect. A: Gen. Atom. Solid State Phys.* **377**(34–36), 1979–1983 (2013).
50. Z. Zhang and Y. Zhang, "Acceleration-level cyclic-motion generation of constrained redundant robots tracking different paths," *IEEE Trans. Syst. Man Cybern. Part B (Cybern.)* **42**(4), 1257–1269 (2012).
51. Y. Zhang, Z. Tan, K. Chen, Z. Yang and X. Lv, "Repetitive motion of redundant robots planned by three kinds of recurrent neural networks and illustrated with a four-link planar manipulators straight-line example," *Robot. Auton. Syst.* **57**(6), 645–651 (2009).
52. S. S. Ge, Y. Zhang and H. L. Tong, "An Acceleration-Based Weighting Scheme for Minimum-Effort Inverse Kinematics of Redundant manipulators, *IEEE International Symposium on Intelligent Control* (2004) pp. 275–280.
53. Y. Zhang, "On the LVI-Based Primal–Dual Neural Network for Solving Online Linear and Quadratic Programming Problems, *American Control Conference*, Portland, OR, USA, vol. 2 (2005) pp. 1351–1356.
54. Y. Zhang, Z. Li, H. Z. Tan and Z. Fan, "On the Simplified LVI-Based Primal–Dual Neural Network for Solving LP and QP Problems," *IEEE International Conference on Control and Automation*, Guangzhou, China (2007) pp. 3129–3134.
55. Z. Zhang, L. Zheng, J. Yu, Y. Li and Z. Yu, "Three recurrent neural networks and three numerical methods for solving a repetitive motion planning scheme of redundant robot manipulators," *IEEE/ASME Trans. Mechatron.* **22**(3), 1423–1434 (2017).

https://doi.org/10.1017/S026357471900119X Published online by Cambridge University Press